Journal of Energy Resources Technology. Received July 09, 2020;
Accepted manuscript posted September 02, 2020. doi:10.1115/1.4048529
Copyright © 2020 by ASME

Check for updates

Effect of buoyancy and inertia on viscoplastic fluid-fluid displacements in a regular and an irregular eccentric annulus

Hans Joakim Skadsem*
University of Stavanger
NORCE Norwegian Research Centre AS / DrillWell
Stavanger, Norway
E-mail: hans.j.skadsem@uis.no

Steinar Kragset
NORCE Norwegian Research Centre AS / DrillWell
Stavanger, Norway

Accepted Manuscript Not Copyedited

Downloaded from http://asmedigitalcollection.asme.org/energyresources/article-pdf/doi/10.1115/1.4048529/6568415/jert-20-1620.pdf by NTNU Universitets Bibliotheket user on 25 September 2020

ABSTRACT

Casing strings and liners are important subsurface structural components in petroleum and in geothermal wells. After the casing string has been run in hole, it is cemented to the formation by pumping a sequence of spacer fluids and cement slurry into the annulus outside the string. Spacer fluids are usually pumped ahead of the cement slurry in order to displace the drilling fluid from the annulus that is to be cemented, and thereby avoid contamination of the cement slurry. Fluid displacements are governed by inertia, buoyancy and viscosity effects, in addition to being strongly influenced by the annular geometry. Poor centralization of the casing or irregularities such as washouts can influence the displacement flows both locally and over long axial distances.

We present three dimensional numerical simulations of the displacement flow involving two viscoplastic fluids in the vicinity of a symmetric local hole enlargement. We focus on laminar flow regimes in the regular part of the annulus and investigate how the volumetric flow rate and the mass density difference between the fluids affect the displacement efficiency in the regular and the irregular parts of the annulus. This study considers viscoplastic displacement flows in a near-vertical, irregular annulus and is an extension of a previous publication that focused on a near-horizontal annulus.

*Address all correspondence to this author.

Journal of Energy Resources Technology. Received July 09, 2020;
Accepted manuscript posted September 02, 2020. doi:10.1115/1.4048529
Copyright © 2020 by ASME

We contextualize our simulations by comparison to industry guidelines for effective and steady laminar displacements in the regular, near-vertical annulus. Here, eccentricity favors flow in the wider sector of the annulus while a positive density difference between the fluids generates secondary, azimuthal flow toward the narrow side of the annulus. In the enlarged and irregular section, both the axial bulk velocity and casing eccentricity decrease sharply and buoyancy becomes more pronounced compared to in the regular annulus. We quantify and discuss the effects of local hole enlargements on displacement efficiencies. Simulations of cementing flows can aid in optimizing fluid properties and pump rates, including when the wellbore has suspected or confirmed zones of irregular geometries.

Downloaded from http://asmedigitalcollection.asme.org/energyresources/article-pdf/doi/10.1115/1.4048529/6568415/jert-20-1620.pdf by NTNU Universitets Biblioteket user on 25 September 2020

Accepted Manuscript Not Copyedited

1 INTRODUCTION

Construction of wells for production of hydrocarbons, geothermal energy or for geological carbon storage proceeds in stages by first drilling a section to a certain target depth, and then securing this section by running a casing string to the bottom of the hole followed by pumping cement slurry into the annular space between casing and formation. Once the cement has hardened, the well construction operation continues by drilling a new and deeper section using a smaller diameter drill bit inside the previously cemented casing. Casing and cement are important structural elements in wells that serve many important functions, including that of providing well integrity and preventing migration or uncontrolled flow of formation fluids along the wellbore.

The operation of cementing casing strings is often referred to as primary cementing and is considered a particularly critical well construction operation. Before primary cementing is performed, the inside and the annular space behind the casing is normally filled by the drilling fluid that was used to drill the current section. In order to cement the space behind casing, cement slurry is conventionally injected down the well inside the casing. Once at the bottom, the cement slurry enters the annulus and flows back up toward the surface, displacing drilling fluid and other fluids ahead of the slurry. The basic fluid displacement process in primary cementing is illustrated in Fig. 1 for a near-vertical hole. The outer casing diameter is slightly smaller than the diameter of the hole, resulting in a narrow annular space, typically of the order of centimeters, that is to be cemented. The geometry of this annular space is often a dominant factor that affects the fluid flow behind casing. As illustrated in the figure, de-centralization or eccentric orientation of the casing in the hole and the possibility of irregularities along the formation wall are particular geometric effects that can have significant impact on the displacement mechanics behind casing. Failure to displace the original drilling fluid from the narrow annular space behind casing can have adverse impacts on well integrity and result in poor zonal isolation along the wellbore. Consequently, the complete displacement of the drilling fluid and minimal inter-mixing between cement slurry and the other fluids are recognized as important criteria for successful primary cementing [1]. As drilling fluids are often yield stress fluids with particles as weighting material that may be hard to displace from narrow annulus geometries, the displacement and cementing operations require careful design of displacing fluid properties, including their mass density and viscosity, and the optimal displacing flow rate.

Partly motivated by the important industrial application of primary cementing, single phase and displacement flows in annular geometries have been investigated for several decades both experimentally and numerically. Eccentric annulus flow

Journal of Energy Resources Technology. Received July 09, 2020;
Accepted manuscript posted September 02, 2020. doi:10.1115/1.4048529
Copyright © 2020 by ASME

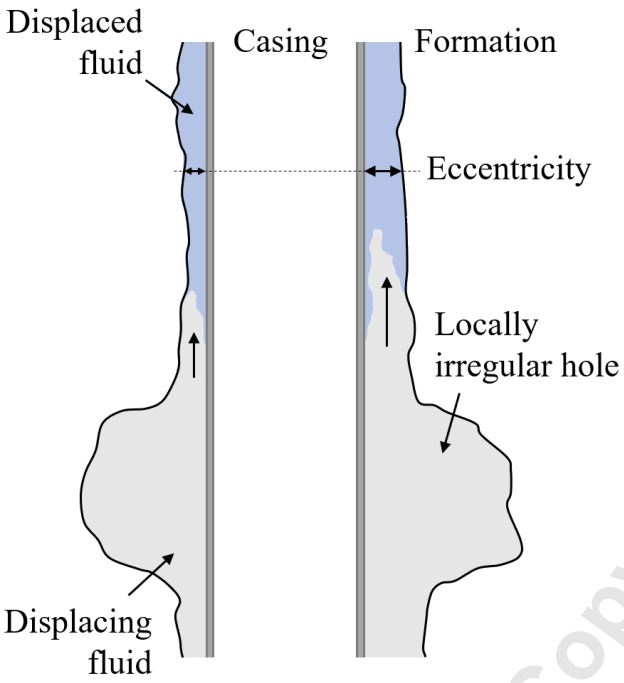

Fig. 1: In conventional primary cementing, the drilling fluid that initially occupies the annular space between casing and the drilled formation is displaced up toward the surface by displacing fluids, including a cement slurry. Fluid flow in the annular space is sensitive to the degree of de-centralization or eccentricity of the casing, and local hole enlargements caused during the drilling process.

of non-Newtonian fluids was investigated by Walton and Bittleston [2] and by Szabo and Hassager [3] who considered a Bingham plastic in a narrow eccentric annulus. They found that eccentricity can cause plugs in the wide and in the narrow sectors of the annulus, and potentially static fluid in the narrow side of the annulus. This can lead to poorly displaced drilling fluid at solid interfaces and potential leakage paths along the cement sheath [4]. Haciislamoglu and Langlinais [5] and Hussain and Sharif [6] have also considered eccentric annulus flow of non-Newtonian shear thinning and yield stress fluids numerically and found that eccentricity promotes flow on the wide side of the annulus and that eccentricity can lead to a significantly reduced axial friction pressure gradient.

Early investigations of annulus displacement and cementing identified the importance of casing eccentricity on the shape of the interface between the two fluids and the displacement quality [7–9]. As pointed out above, the casing string to be cemented is in practice always de-centralized in the hole, even in vertical wellbores [10], and this results in higher flow velocities in the wide sector of the annulus compared to the narrow sector. Unless compensated for by density and/or viscosity contrasts between displaced and displacing fluids, eccentricity will cause the fluid-fluid interface to elongate axially and give poor displacement on the narrow side of the annulus. More recent laboratory measurements such as those reported by Jakobsen *et al.* [11], Tehrani *et al.* [12] and Malekmohammadi *et al.* [13] have improved the fundamental fluid mechanics insight into vertical and inclined annulus displacement flows, including the existence of secondary azimuthal flows from the wide to the narrow side of an eccentric annulus and the existence of steady, laminar displacement flows.

To guide fluid and job design toward more effective laminar displacements, industry-accepted guidelines have been

Accepted Manuscript Not Copyedited

Downloaded from http://asmedigitalcollection.asme.org/energyresources/article-pdf/doi/10.1115/1.4048529/6568415/jert-20-1620.pdf by NTNU Universitets Biblioteket user on 25 September 2020

Journal of Energy Resources Technology. Received July 09, 2020;
Accepted manuscript posted September 02, 2020. doi:10.1115/1.4048529
Copyright © 2020 by ASME

developed. An example of such a rule set is the *effective laminar flow* (ELF) guidelines [14–16] which state that:

1. The displacing fluid should be at least 10 % heavier than the displaced fluid,
2. The friction pressure gradient exerted by the displacing fluid should be at least 20 % larger than that of the displaced fluid,
3. The shear stress on the narrow side of the annulus must exceed the yield stress of the displaced fluid, and
4. The flow resistance of the displacing fluid on the wide side of the annnulus must be larger than that of the displaced fluid on the narrow side.

The first two ELF rules ensure density and viscosity hierarches between the fluids, so that the denser and more viscous fluid is the displacing fluid which should be underneath the lighter and less-viscous displaced fluid in a near-vertical annulus. The third rule ensures mobiliziation of the fluid to be displaced, while the fourth rule promotes a stable shape of the fluid interface in vertical and inclined annuli.

The applicability of the ELF rules was investigated by Pelipenko and Frigaard [16], using a lubrication model derived from the two-dimensional gap-averaged displacement model of Bittleston *et al.* [17]. Their results show that the ELF rules are generally more conservative than the lubrication model predictions when it comes to steady state displacements, *i.e.* the lubrication model predicts good displacement conditions for some parameter combinations where the ELF rules are not satisfied.

Most of the work discussed above have focused on displacement flows in annuli with regular cross sections or slowly varying geometric features. As shown by caliper logs, and as indicated in Fig. 1, wellbores can exhibit a wide variety of irregular shapes resulting from *e.g.* the drilling process itself or the existence of weak or unconsolidated formation layers [18, 19]. For shales in particular, chemical interaction between drilling fluid and formation can lead to wellbore instability problems and irregular wellbore geometries [20, 21]. The single phase flow of yield stress (Bingham plastic) fluids in annuli with axisymmetric cavities was recently investigated numerically by Roustaei *et al.* [22–24]. The work was motivated by drilling fluid conditioning ahead of displacement and cement placement. The studies showed that fluid can remain unyielded inside washout sections and the existence of a generally non-linear relation between Reynolds number and the circulating area of the irregularity [23, 24].

Relatively few studies have addressed displacement flows in annuli with hole enlargements or similar sudden changes to the flow path. Yard tests such as Refs. [8, 25–27] have investigated the effect of sudden hole enlargements on the hardened cement quality. More recently, laboratory measurements on displacement flows in a nearly horizontal irregular annulus were reported by Lund *et al.* [28] and analyzed further by numerical simulation by Renteria *et al.* [29] and Skadsem *et al.* [30]. Additional numerical simulations of displacement in irregular slanted and near-horizontal annuli were presented by Kragset and Skadsem [31]. The simulations showed that the displacement flow becomes fully three-dimensional inside the enlargement, and that the displacement is mainly governed by the balance between buoyancy and inertia forces.

The brief overview above suggests that annulus displacements from irregular geometries have so far primarily been studied in near-horizontal annuli. As buoyancy, and therefore inclination, is considered important for fluid displacement

Accepted Manuscript Not Copyedited

Downloaded from http://asmedigitalcollection.asme.org/energyresources/article-pdf/doi/10.1115/1.4048529/6568415/jert-20-1620.pdf by NTNU Universitets Biblioteket user on 25 September 2020

Journal of Energy Resources Technology. Received July 09, 2020;
Accepted manuscript posted September 02, 2020. doi:10.1115/1.4048529
Copyright © 2020 by ASME

of irregular annuli, we turn our attention in this paper to cementing of *near-vertical* casing strings and investigate non-Newtonian fluid displacements in an eccentric annulus with a sudden hole enlargement using *fully 3D* numerical simulations. Very recently, Etrati *at al.* [32], considered vertical wellbores and the displacement of yield stress drilling fluids by Newtonian spacer fluids from the annular space outside surface casings. For a sudden hole enlargement, as we also study in this paper, Etrati *et al.* found that for sufficiently high Reynolds numbers, the flow destabilizes inside the washout resulting in fluid inter-mixing and recirculation that may improve the overall displacement of the washout volume. Further, buoyancy was seen to improve overall mud removal from the washout, especially in the viscous-dominated regime, as the density difference helps move the displacing spacer fluid laterally in the washout [32]. Our results are considered novel and complementary to those reported by Etrati *et al.* as we resolve the full three-dimensional flow field in near-vertical, irregular annuli involving two non-Newtonian fluids. Further, we compare displacements in a regular eccentric annulus to that of an eccentric annulus with a sudden hole enlargement, and assess our results on the basis of the ELF design rules. Results presented in these studies can help improve fluid design and operational planning for cementing of casings that penetrate known or expected irregular layers. Insights from these studies can also benefit other industries for which fluid displacement from non-uniform geometry process equipment is relevant.

The structure of this paper is as follows: We begin by defining the governing equations, the annulus geometry under consideration and the fluid properties in the next section. We proceed by evaluating the design rules and stability conditions for the specific cases investigated in this paper. We next turn to validation of the 3D numerical simulations based on displacement efficiency measurements from a vertical, eccentric annulus, followed by presentation and discussion of our main observations. Finally, we summarize and draw conclude.

PROBLEM DEFINITION

We consider isothermal and laminar flow of shear thinning yield stress fluids in an annulus geometry with and without a local hole enlargement. The annulus *with* a local hole enlargement is shown in Fig. 2, where the left panel provides a close-up of the irregular section with some parts clipped away for illustration. The middle panel provides a view of the entire length of the annulus geometry, which we assume is inclined by 5° from the vertical, as indicated by comparison with the vertical direction represented by the black arrow in the right panel. The main geometric features and dimensions are summarized in Table 1. In addition to the irregular geometry shown in Fig. 2, we also present results from a regular annulus without the enlarged, washout section. In all cases we take inner-pipe eccentricity in the regular sections to be 42 %, with the narrow part of the annulus toward the lower side of the annulus. As shown by Guillot *et al.* [10], even in near-vertical wellbores, this level of eccentricity is realistic and relevant for primary cementing operations.

We assume that the rheological properties of both the displaced fluid and the displacing fluid can be approximated by

Accepted Manuscript Not Copyedited

Downloaded from http://asmedigitalcollection.asme.org/energyresources/article-pdf/doi/10.1115/1.4048529/6568415/jert-20-1620.pdf by NTNU Universitets Biblioteket user on 25 September 2020

Journal of Energy Resources Technology. Received July 09, 2020;
Accepted manuscript posted September 02, 2020. doi:10.1115/1.4048529
Copyright © 2020 by ASME

Table 1: Physical dimensions of the annular geometry.

Dimension	Value (mm)
Outer radius, regular annulus, R_o	115.32
Outer radius, washout	195.16
Annulus inner radius, R_i	88.90
Offset between cylinder axes, δ	11.10
Inlet axial length	12000
Washout taper axial length	67.05
Washout axial length	2319
Washout taper axial length	67.05
Outlet axial length	21550

Fig. 2: The model geometry of a 36 m eccentric annulus with an irregular section. The geometry is inclined from the vertical (black arrow) by 5°. A close-up of the irregular section with some parts clipped away for visibility is shown to the left. In all cases, the narrow side of the annulus is toward the lower side of the annulus.

the Herschel-Bulkley model

$$\dot{\boldsymbol{\gamma}} = 0, \qquad \text{where } \tau \leq \tau_y, \tag{1a}$$

$$\boldsymbol{\tau} = \mu(\dot{\gamma})\dot{\boldsymbol{\gamma}}, \qquad \text{elsewhere}, \tag{1b}$$

Accepted Manuscript Not Copyedited

Downloaded from http://asmedigitalcollection.asme.org/energyresources/article-pdf/doi/10.1115/1.4048529/6568415/jert-20-1620.pdf by NTNU Universitets Biblioteket user on 25 September 2020

Journal of Energy Resources Technology. Received July 09, 2020;
Accepted manuscript posted September 02, 2020. doi:10.1115/1.4048529
Copyright © 2020 by ASME

where $\dot{\boldsymbol{\gamma}}$ denotes the rate-of-strain tensor and the viscosity function is defined as $\mu(\dot{\gamma}) = \tau_y/\dot{\gamma} + K\dot{\gamma}^{n-1}$. Here, the yield stress is denoted τ_y, K is the consistency index and the shear thinning index is $n \leq 1$.

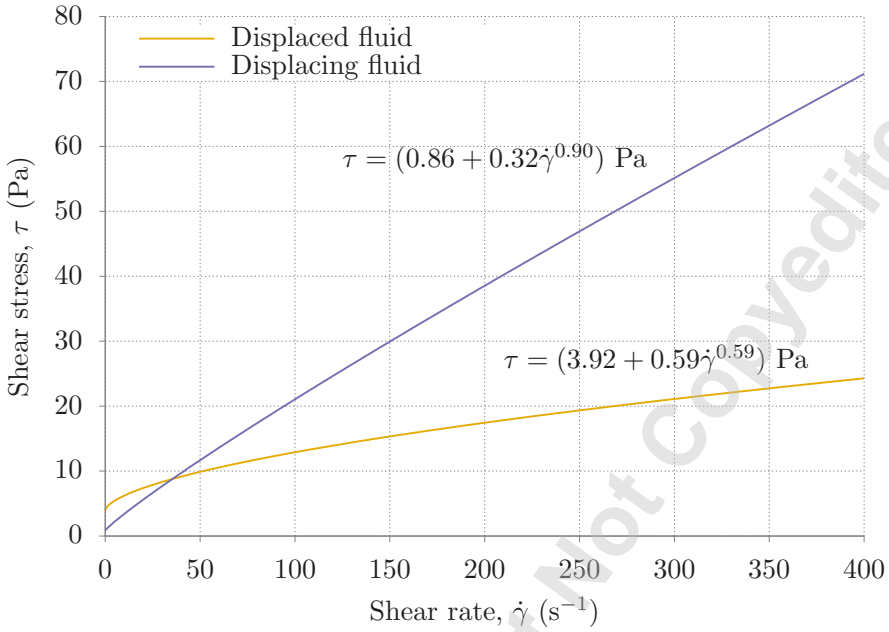

Fig. 3: Flow curves for displaced and displacing fluid.

We base the Herschel-Bulkley model parametrizations of the displaced and the displacing fluids on six- and eight-speed viscometer measurements of a conventional polymeric water-based drilling fluid and a conventional oil-well cement slurry, respectively. To be specific, we assume the displaced fluid is approximated by $\tau = (3.92 + 0.59\dot{\gamma}^{0.59})$ Pa, while the displacing cement slurry is represented by $\tau = (0.86 + 0.32\dot{\gamma}^{0.9})$ Pa, based on measurements from a previous full-scale cementing experiment [33]. Flow curves for the displaced and displacing fluids are plotted in Fig. 3. As for the density, we take the mass density of the displacing fluid to be based on conventional cement slurries, fixed at 1.92 s.g. The density of the displaced fluid is varied in order to assess the importance of buoyancy and taken as either 1.5 s.g. or 1.8 s.g. in the simulations. Although increasing the density of the displaced fluid from 1.5 s.g. to 1.8 s.g. would affect the viscosity of the fluid, we assume for simplicity that the same Herschel-Bulkley model parameters apply irrespective of mass density. Finally, we note that these fluid parametrizations are identical to those in a previous paper on displacements in a near-horizontal, irregular annulus geometry [31]. As for the injection rate, we will consider constant rates of either 150 l/min or 900 l/min in order to vary the effective viscosity hierarchy between the fluids.

The governing equations for each of the two fluid phases are derived from the principles of mass and momentum

Accepted Manuscript Not Copyedited

Downloaded from http://asmedigitalcollection.asme.org/energyresources/article-pdf/doi/10.1115/1.4048529/6568415/jert-20-1620.pdf by NTNU Universitets Biblioteket user on 25 September 2020

Journal of Energy Resources Technology. Received July 09, 2020;
Accepted manuscript posted September 02, 2020. doi:10.1115/1.4048529
Copyright © 2020 by ASME

conservation which result in the two equations:

$$\nabla \cdot \mathbf{u} = 0, \tag{2}$$

$$\rho\left(\frac{\partial \mathbf{u}}{\partial t} + \mathbf{u}\cdot\nabla\mathbf{u}\right) = -\nabla p + \nabla\cdot\boldsymbol{\tau} + \rho\mathbf{g}. \tag{3}$$

Here ρ is the fluid mass density, $\mathbf{u}$ is the three dimensional velocity field, p is pressure, $\boldsymbol{\tau}$ is the deviatoric stress tensor and $\mathbf{g}$ is the gravitational acceleration. Gravity is the only body force present in these simulations.

The governing equations are solved using the open-source computational fluid dynamics platform OpenFOAM ver. 5.0 [34] and the volume of fluid approach where the fluids are treated as immiscible and with no surface tension. We specify for the velocity Dirichlet conditions at solid boundaries and at the inlet (no slip and uniform, bulk inlet velocity, respectively) and a Neumann outflow condition at the outlet. For the pressure, Neumann inlet and Dirichlet outlet conditions are used. In our numerical simulations, the viscosity is regularized using the Papanastasiou regularization [35] to ensure a finite viscosity also at zero shear rate, *viz.* Eq. (1b) is applied everywhere with the regularized viscosity function $\mu(\dot{\gamma}) = \tau_y[1-\exp(-m\dot{\gamma})]/\dot{\gamma} + K\dot{\gamma}^{n-1}$.

DIMENSIONAL ANALYSIS

We now characterize the parameter combinations in the simulations using dimensionless numbers that are representative for the eccentric annulus displacement flows. We first introduce the concentric annulus gap width $d^* = 2(R_o - R_i)$ as a characteristic length scale and take the axial bulk velocity Q/A to be the velocity scale U^*. Further, we let $\dot{\gamma}^* = 4U^*/d^*$ be the characteristic shear rate and $\mu_i^* = \tau_{y,i}/\dot{\gamma}^* + K_i\dot{\gamma}^{*n_i-1}$ be the characteristic viscosity of fluid i. Based on these scales, we define the dimensionless numbers in Table 2 as characteristic dimensionless numbers for the flows investigated in this paper. The ratio of inertia to viscous forces for fluid i is characterized by the Reynolds number Re_i, the ratio of yield stress

Table 2: Dimensionless numbers for scaling analysis.

Number	Definition	Description
κ	R_i/R_o	Pipe radius ratio
e	$\delta/(R_o-R_i)$	Eccentricity
At	$\frac{\rho_2-\rho_1}{\rho_1+\rho_2}$	Atwood number
Re_i	$\frac{\rho_i U^* d^*}{\mu_i^*}$	Reynolds number for fluid i
Bn_i	$\frac{\tau_{y,i} d^*}{\mu_i^* U^*}$	Bingham number for fluid i
Fr	$\frac{U^*}{\sqrt{Atgd^*}}$	Froude number
n_i		Shear thinning index for fluid i

Accepted Manuscript Not Copyedited

Downloaded from http://asmedigitalcollection.asme.org/energyresources/article-pdf/doi/10.1115/1.4048529/6568415/jert-20-1620.pdf by NTNU Universitets Biblioteket user on 25 September 2020

Journal of Energy Resources Technology. Received July 09, 2020;
Accepted manuscript posted September 02, 2020. doi:10.1115/1.4048529
Copyright © 2020 by ASME

to viscous stresses is given by the Bingham number Bn_i and the densimetric Froude number Fr expresses the ratio of inertia to buoyancy forces. Here, and in the following, we denote the displacing fluid as $i = 1$ and the displaced fluid as $i = 2$.

An overview of key dimensionless numbers for the four cases we consider is provided in table 3.

Table 3: Summary of main dimensionless numbers.

Simulation	Re_2	Re_1	Bn_2	Fr
$\rho_2 = 1.5$ s.g., $Q = 150$ l/min	20	46	2.5	0.6
$\rho_2 = 1.5$ s.g., $Q = 900$ l/min	428	403	1.4	3.5
$\rho_2 = 1.8$ s.g., $Q = 150$ l/min	25	46	2.5	1.1
$\rho_2 = 1.8$ s.g., $Q = 900$ l/min	514	403	1.4	6.8

At the lowest flow rate of 150 l/min, the Reynolds numbers for the 1.5 sg and 1.8 sg displaced fluid are estimated to be 20 and 25, and 46 for the displacing fluid. At the highest flow rate of 900 l/min, the displaced fluid Reynolds numbers are 428 and 514 for 1.5 sg and 1.8 sg density fluid, respectively. The displacing fluid is effectively more viscous at this flow rate, resulting in a lower Reynolds number of 403. In all cases, these Reynolds numbers suggest laminar conditions. The Bingham numbers are larger for the displaced fluid compared to the displacing fluid (2.5 and 1.4 at respectively 150 l/min and 900 l/min, compared to 0.9 and 0.2 for the displacing fluid at the same flow rates). The densimetric Froude number varies from a minimum of 0.6 at a flow rate of 150 l/min with 1.5 sg. displaced fluid (buoyancy most prominent relative to inertia) and up to 6.8 at 900 l/min and 1.8 sg. displaced fluid (buoyancy least prominent relative to inertia). While the Reynolds numbers considered here are comparable to the simulations by Etrati *et al.* [32], the Bingham numbers in our study are consistently smaller, suggesting smaller yield stress effects compared to their recent study. Finally, the density differences in our study range from approximately 7 % to more than 2 %, overlapping with the density difference of up to 8 % in Ref. [32]. Concerning the effect of buoyancy as expressed by the densimetric Froude number, certainly the cases with the lowest flow rate stand out among the cases listed in table 3.

EFFECTIVE LAMINAR FLOW GUIDELINES

In the following we will evaluate the ELF design rules proposed by Couturier *et al.* [14] and presented in the introduction of this paper.

Rule 1: Density hierarchy

The displacing fluid mass density is 1.92 s.g. in our simulations. In order to meet the density hierarchy requirement presented in the introduction, the mass density of the displaced fluid should not exceed 1.75 s.g. This rule is satisfied for the lightest displaced fluid (mass density 1.5 s.g.), but violated for the 1.8 s.g. displaced fluid.

Accepted Manuscript Not Copyedited

Downloaded from http://asmedigitalcollection.asme.org/energyresources/article-pdf/doi/10.1115/1.4048529/6568415/jert-20-1620.pdf by NTNU Universitets Biblioteket user on 25 September 2020

Journal of Energy Resources Technology. Received July 09, 2020;
Accepted manuscript posted September 02, 2020. doi:10.1115/1.4048529
Copyright © 2020 by ASME

Rule 2: Friction pressure hierarchy

To determine the minimum flow rate required to achieve the recommended viscosity hierarchy in a regular, concentric annulus with the dimensions specified above, we use the semianalytical solution presented by Hanks [36] to predict the relation between flow rate and pressure gradient for the two fluids. The fully developed, laminar results are shown in Fig. 4. For flow rates above approximately 300 l/min, we meet the friction pressure hierarhcy requirement stated in the introduction.

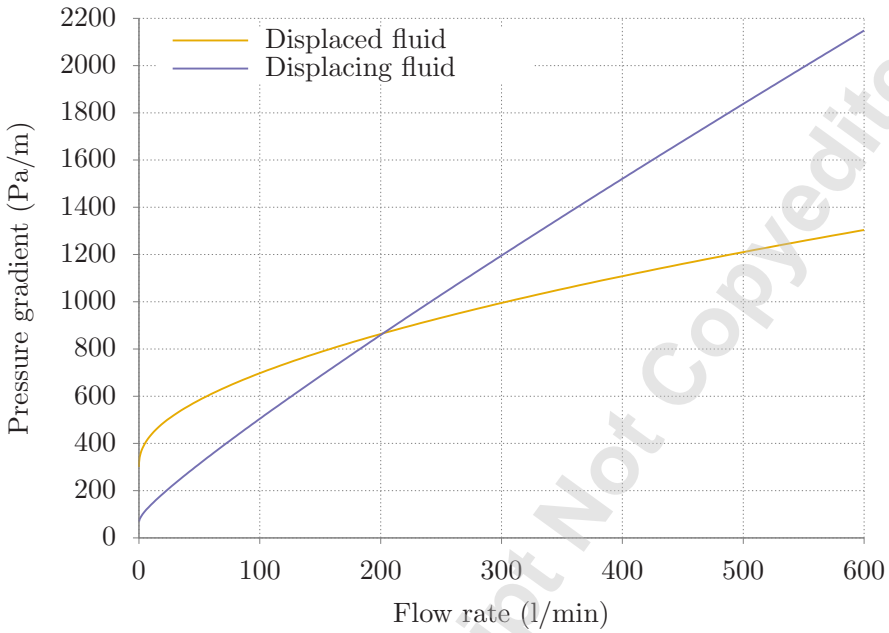

Fig. 4: Pressure gradient and flow rate in the concentric annulus.

Thus, at the low flow rate of 150 l/min in our simulations, we violate the friction pressure hierarchy between the two fluids. At 900 l/min, the displacing fluid exerts a friction pressure gradient that is significantly higher than that of the displaced fluid.

Rule 3: Mobilization on narrow side

This requirement can be expressed as follows [15]:

$$\left(\frac{dp}{dL}\right)_1 + (\rho_1 - \rho_2) g \cos\beta > \frac{2\tau_{y,2}}{h},$$

where subscript 1 refers to displacing fluid and subscript 2 to displaced fluid. Further, $(dp/dL)_1$ is the friction pressure gradient of the displacing fluid evaluated in an equivalent concentric annulus, β is the inclination from vertical and h is the radial gap on the narrow side of the eccentric annulus. Considering an eccentricity of $e = 0.42$, we find that the radial gap on the narrow side of the annulus is $h = (1-e)(r_o - r_i) \approx 0.015$ m, so that $2\tau_{y,2}/h \approx 512$ Pa/m. This is balanced by a hydrostatic pressure difference $(\rho_1 - \rho_2)g$ with $\rho_2 \approx 1.87$ s.g. in a vertical annulus when $\rho_1 = 1.92$ s.g. Consequently, mobilization

Accepted Manuscript Not Copyedited

Downloaded from http://asmedigitalcollection.asme.org/energyresources/article-pdf/doi/10.1115/1.4048529/6568415/jert-20-1620.pdf by NTNU Universitets Biblioteket user on 25 September 2020

Journal of Energy Resources Technology. Received July 09, 2020;
Accepted manuscript posted September 02, 2020. doi:10.1115/1.4048529
Copyright © 2020 by ASME

of displaced fluid on the narrow side of the annulus is ensured for both of the displaced fluids in our simulations since the maximum density we consider is 1.8 s.g.

Rule 4: Differential velocity

The final rule is formulated to ensure that the displacing fluid is not flowing faster in the wide sector of the annulus than the axial velocity of the displaced fluid in the narrow sector of the annulus. The rule can be expressed mathematically as follows [15, 16]:

$$\left(\frac{dp}{dL}\right)_1^{\text{wide}} + \rho_1 g\cos\beta > \left(\frac{dp}{dL}\right)_2^{\text{narrow}} + \rho_2 g\cos\beta, \tag{4}$$

where $(dp/dL)_1^{\text{wide}}$ is the friction pressure gradient of the displacing fluid in a concentric annulus with gap width equivalent to that of the wide side of the original, eccentric annulus at the same bulk velocity as the original problem. Similarly, $(dp/dL)_2^{\text{narrow}}$ is the friction pressure gradient of the displaced fluid in a concentric annulus with gap width equal to that of the narrow side of the original annulus.

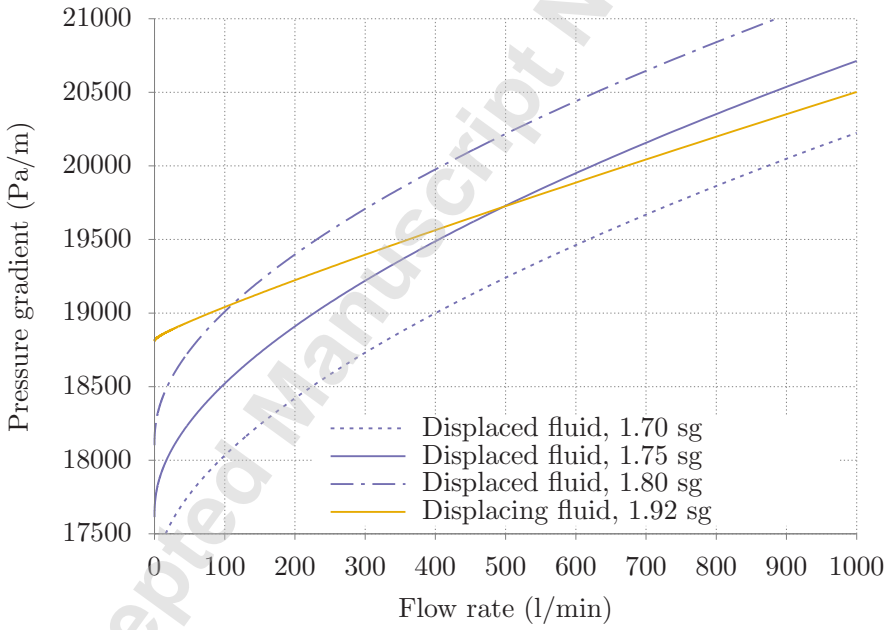

Fig. 5: Evaluation of the differential velocity rule, Eq. (4) for the displaced and displacing fluid rheologies and two different mass densities of the displaced fluid. The lines correspond to the sum of the friction pressure gradient and the hydrostatic component for each of the fluids.

In Fig. 5 we evaluate the differential velocity criterion (4) for the displacing fluid with mass density 1.92 s.g. and the displaced fluid at three different mass densities. The lines correspond to the sum of the friction pressure gradient and the hydrostatic term, evaluated for a near-vertical annulus inclined by 5° from the vertical.

Accepted Manuscript Not Copyedited

Downloaded from http://asmedigitalcollection.asme.org/energyresources/article-pdf/doi/10.1115/1.4048529/6568415/jert-20-1620.pdf by NTNU Universitets Biblioteket user on 25 September 2020

Journal of Energy Resources Technology. Received July 09, 2020;
Accepted manuscript posted September 02, 2020. doi:10.1115/1.4048529
Copyright © 2020 by ASME

Table 4: Summary of ELF design rule evaluation.

Simulation	Rule 1	Rule 2	Rule 3	Rule 4
$\rho_2 = 1.5$ s.g., $Q = 150$ l/min	✓	✗	✓	✓
$\rho_2 = 1.5$ s.g., $Q = 900$ l/min	✓	✓	✓	✓
$\rho_2 = 1.8$ s.g., $Q = 150$ l/min	✗	✗	✓	✗
$\rho_2 = 1.8$ s.g., $Q = 900$ l/min	✗	✓	✓	✗

We summarize the discussion above in Table 4, where we indicate which combinations of displaced fluid mass density and injection rates that satisfy each of the four ELF design rules.

RESULTS

Above we have evaluated the four different combinations of displaced fluid mass density and flow rate against the ELF rules designed to promote steady, effective laminar displacements. We now turn to results from 3D computational fluid dynamics simulations. In this section we will first assess the accuracy of the numerical method before we present 3D simulation results of the four cases under study, for both a regular, eccentric annulus and for an eccentric annulus with the irregular section shown in Fig. 2.

Model validation

We begin this section by assessing the accuracy of the numerical method by comparing simulation results to experimental data presented by Tehrani et al. [12, 37], which was also used by Tardy and Bittleston [38] who included additional experimental results that was not presented in [12]. In the experiments we use for model validation, a yield stress fluid is displaced from a vertical, eccentric annulus by another yield stress fluid with the same effective viscosity and equal or higher mass density. The viscosity of both fluids are characterized by the Herschel–Bulkley parametrization $\tau = (1.52 + 0.246\dot{\gamma}^{0.509})$ Pa and the density of the displacing fluid varies from 0 to 16.77 % higher than that of the displaced fluid [38]. Based on fluid property information in Ref. [37], we approximate the mass density of the displaced fluid to be $\rho = 1000$ kg/m^3. The annulus under consideration is 3 m long and has outer radius 0.025 m and inner radius 0.02 m, with eccentricity 50 %. The flow rate is 2.5×10^{-4} m^3/s, corresponding to a bulk velocity of approximately 0.3537 m/s [38].

We compare numerical simulations of *displacement efficiencies* to experimental measurements which we have extracted from Ref. [38]. Displacement efficiency can best be defined by considering an annular volume V_0 that is initially filled with a fluid that is flowing axially at a constant volumetric rate Q. Then, at $t = 0$, a displacing fluid (that may be the same or a different fluid) is suddenly introduced at the inlet to V_0. The displacement efficiency at a time t, $E(t)$, is then defined as the volume inside V_0 occupied by the displacing fluid relative to the total volume V_0. To facilitate the result presentation, we will use a dimensionless time $t^* = Qt/V_0$ to compare results from the displacement simulations with the experimental measurements. Thus, at $t^* = 1$, all the initial fluid is displaced from the annulus if perfect displacement is achieved in any of

Accepted Manuscript Not Copyedited

Downloaded from http://asmedigitalcollection.asme.org/energyresources/article-pdf/doi/10.1115/1.4048529/6568415/jert-20-1620.pdf by NTNU Universitets Biblioteket user on 25 September 2020

Journal of Energy Resources Technology. Received July 09, 2020;
Accepted manuscript posted September 02, 2020. doi:10.1115/1.4048529
Copyright © 2020 by ASME

the simulations [12].

In Fig. 6 simulation results with meshes ranging from 10^4 to 4×10^6 cells are shown for the case with the largest density difference, $\Delta\rho/\rho = 16.77$ %, between the two fluids. This seemed to be the most demanding case due to the secondary (azimuthal) flows produced by the buoyancy forces. Various combinations of azimuthal, radial and axial resolution were tested and the bundle of lines indicates the spread of the results. The solid dots show the results of a relatively coarse resolution with 5×10^4 cells that was eventually chosen for the remaining parts of this study as this produced satisfactory accuracy for the qualitative assessments in the current work. The other cases with smaller density differences are shown in Fig. 7, and the agreement can be seen to be good between the simulations and the experimental measurements for these cases.

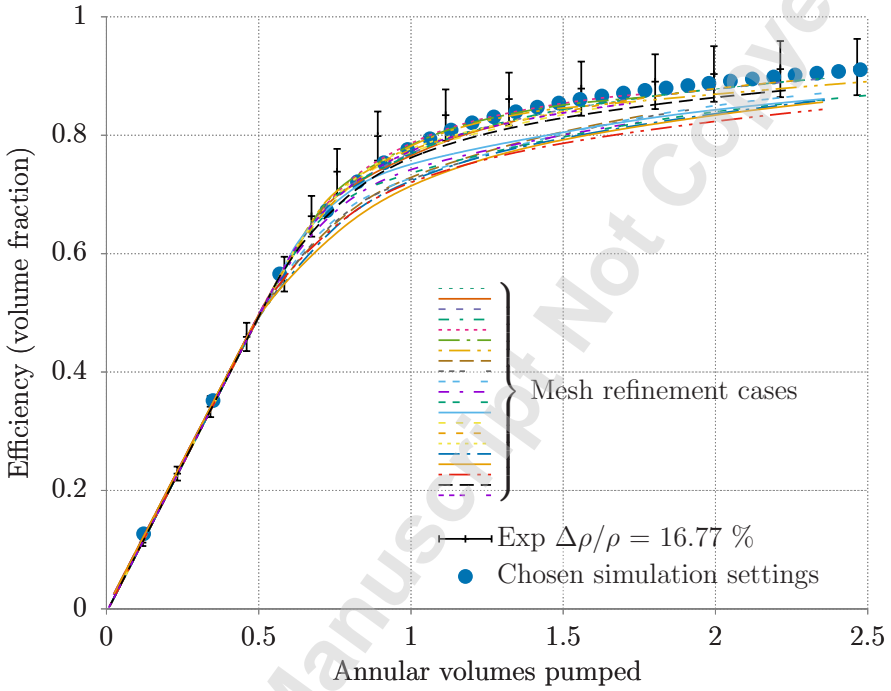

Fig. 6: Comparison of displacement efficiency results from simulations and experimental measurements (points with error bars) of Tehrani et al. [12, 37, 38]. The bundle of lines shows results from mesh refinement variations, and the solid dots indicate simulations with settings finally chosen for the remaining part of this study.

Regular annulus

In Fig. 8 we plot the volume fraction of non-displaced fluid at time $t^* = 0.5$, averaged over the annulus cross section as function of axial position. The top and bottom panel corresponds to displaced fluid mass densities 1.8 s.g. and 1.5 s.g., respectively. From the bottom panel, we observe a clear transition from mainly displacing fluid at axial positions below 18 m, to mainly displaced fluid above. The transition occurs over a short axial length, corresponding to nearly piston-like displacement at both flow rates at this density difference. The total axial length of our geometry is 36 m, so the transition

Accepted Manuscript Not Copyedited

Downloaded from http://asmedigitalcollection.asme.org/energyresources/article-pdf/doi/10.1115/1.4048529/6568415/jert-20-1620.pdf by NTNU Universitets Biblioteket user on 25 September 2020

Journal of Energy Resources Technology. Received July 09, 2020;
Accepted manuscript posted September 02, 2020. doi:10.1115/1.4048529
Copyright © 2020 by ASME

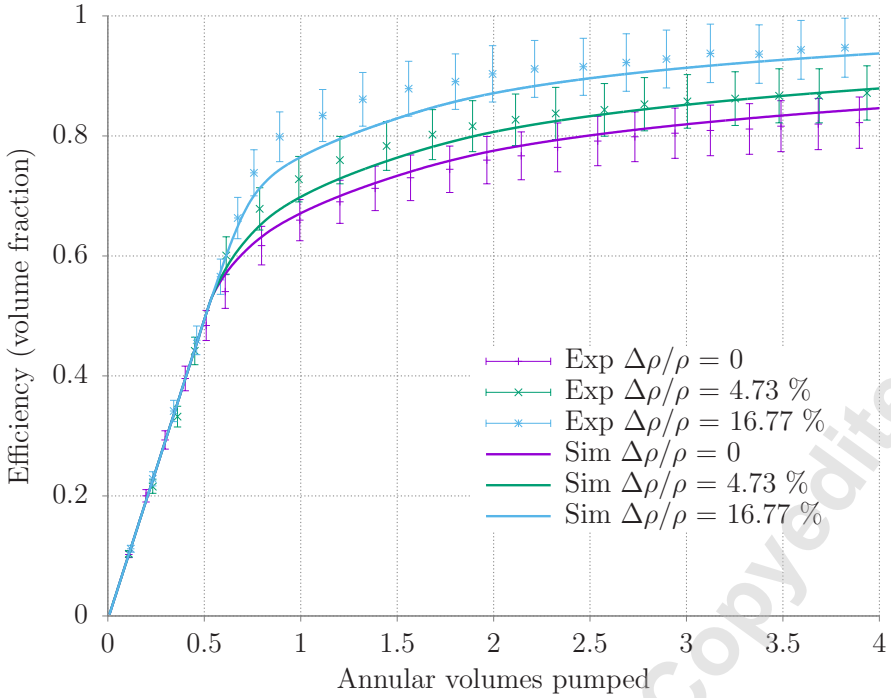

Fig. 7: Comparison of displacement efficiency results from simulations (lines) and experimental measurements (points with error bars) of Tehrani et al. [12, 37, 38].

occurs at approximately 18 m, as expected for piston-like displacements at $t^* = 0.5$. In the top panel where the density difference and buoyancy is reduced, we observe a more gradual transition.

To obtain a better impression of residual fluid distribution along the regular annulus, we plot the volume fraction of non-displaced fluid averaged separately over the wide and the narrow sides in Figs. 9 and 10 for each of the cases we consider. From the bottom panels of Figs. 9 and 10 we see that the larger density difference (1.5 s.g. vs. 1.92 s.g.) clearly promotes a more piston-like displacement compared to the top panels where the density difference is smaller (1.8 s.g. vs. 1.92 s.g.). Buoyancy is effective in displacing fluid from the narrow side of the annulus, especially at the lowest flow rate (Fig. 9). Again, at $t^* = 0.5$ the transition from displacing fluid to displaced fluid occurs at an axial position of approximately 17 - 18 m, corresponding to approximately 50 % of the axial length of our geometry. The top panels show a larger axial elongation of the transition region between displacing and displaced fluid, and also much larger differences between the narrow and the wide side of the annulus. These results underline the importance of buoyancy (mass density difference) for effective displacements in near-vertical and eccentric annuli.

Finally, in Fig. 11 we plot the distribution of displacing (blue) fluid after injecting a displacing fluid volume corresponding to 50 % of the annulus volume, *i.e.* $t^* = 0.5$, for each of the four cases under consideration. A displacing fluid volume fraction of 10 % corresponds to the brightest blue color; darkest blue corresponds to 100% volume fraction displacing fluid. The displaced fluid is made transparent in order to facilitate the three dimensional visualization. Averaging the fluid distributions in Fig. 11 over the entire annulus cross section or separately across the wide and narrow parts of the annulus reproduces Fig. 8 and Figs. 9 and 10, respectively.

Accepted Manuscript Not Copyedited

Downloaded from http://asmedigitalcollection.asme.org/energyresources/article-pdf/doi/10.1115/1.4048529/6568415/jert-20-1620.pdf by NTNU Universitets Biblioteket user on 25 September 2020

Journal of Energy Resources Technology. Received July 09, 2020;
Accepted manuscript posted September 02, 2020. doi:10.1115/1.4048529
Copyright © 2020 by ASME

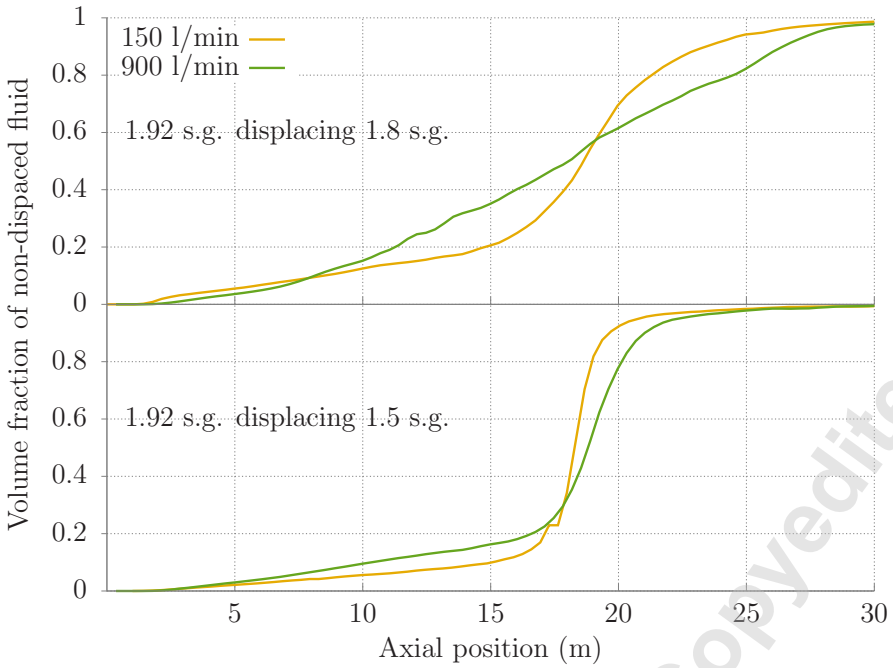

Fig. 8: The cross-sectional average of the non-displaced volume fraction at $t^* = 0.5$ as a function of the axial position in the regular annulus model. The density of the displaced fluid is varied between 1.5 s.g. and 1.8 s.g. while the displacing fluid is kept at 1.92 s.g. in all the cases. Two different flow rates are considered for each combination of mass densities.

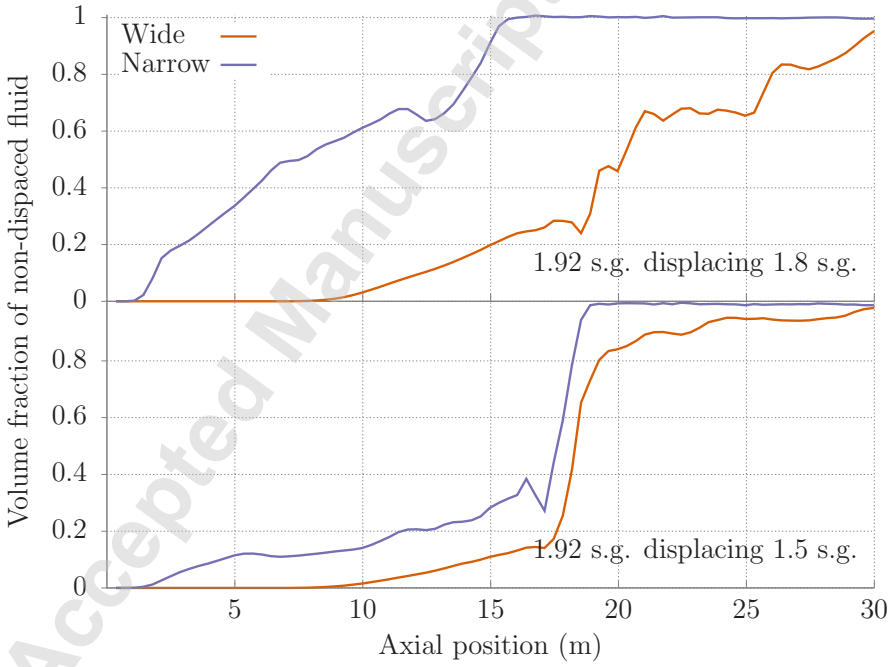

Fig. 9: Averages of the non-displaced volume fraction across the wide (red) and the narrow (blue) gaps, respectively, at $t^* = 0.5$ as a function of the axial position in the regular annulus model. The density of the displaced fluid is varied between 1.5 s.g. and 1.8 s.g. while the displacing fluid is kept at 1.92 s.g. in all the cases. The flow rate is 150 l/min.

Accepted Manuscript Not Copyedited

Downloaded from http://asmedigitalcollection.asme.org/energyresources/article-pdf/doi/10.1115/1.4048529/6568415/jert-20-1620.pdf by NTNU Universitets Biblioteket user on 25 September 2020

Journal of Energy Resources Technology. Received July 09, 2020;
Accepted manuscript posted September 02, 2020. doi:10.1115/1.4048529
Copyright © 2020 by ASME

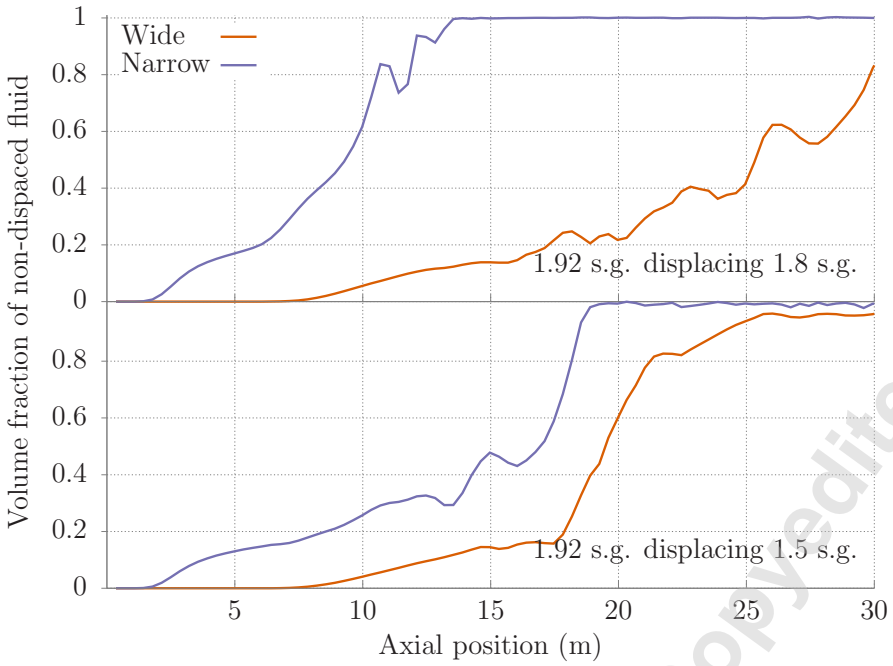

Fig. 10: Averages of the non-displaced volume fraction across the wide (red) and the narrow (blue) gaps, respectively, at $t^* = 0.5$ as a function of the axial position in the regular annulus model. The density of the displaced fluid is varied between 1.5 s.g. and 1.8 s.g. while the displacing fluid is kept at 1.92 s.g. in all the cases. The flow rate is 900 l/min.

Irregular annulus

We next turn our attention to displacements in the irregular annulus geometry with a sudden washout section. In Fig. 12 we show cross-sectional averages of the volume fraction of the non-displaced fluid at $t^* = 1$ as function of axial position. The washout is indicated by the colored region in these plots, and we note that the volume fraction is measured relative to the local cross-sectional area times a differential length. This means that the absolute volume of non-displaced fluid within the washout is larger than it appears when compared to the regular parts due to the difference between the cross-sectional areas of the regular sections and the washout.

Consistent with the results of Etrati *at al.* [32], we note by comparing the two panels that increasing the mass density difference between the fluids improves the displacement efficiency. We begin by considering the lower panel, where, at $t^* = 1$, there is nearly no residual non-displaced fluid below the washout section for either flow rate. Inside the washout, the lower flow rate leads to improved displacement of the lighter 1.5 s.g. fluid. Etrati *et al.* also found significant improvements in the displacement efficiency due to buoyancy especially at lower Reynolds numbers and in the viscous dominated regime. Above the washout, the lower flow rate leads to markedly lower volume fraction of non-displaced fluid and apparently improved displacement efficiency compared to the case of 900 l/min pump rate. We next turn our attention to the top panel in Fig. 12. Inside the washout section in particular, the lower flow rate of 150 l/min is again more effective in displacing the irregular section. Based on the evaluation at $t^* = 1$ in Fig. 12, the combination of low mass density difference (1.8 s.g. vs. 1.92 s.g.) and high flow rate (900 l/min) results in the overall poorest displacement of these four cases.

Accepted Manuscript Not Copyedited

Downloaded from http://asmedigitalcollection.asme.org/energyresources/article-pdf/doi/10.1115/1.4048529/6568415/jert-20-1620.pdf by NTNU Universitets Biblioteket user on 25 September 2020

Journal of Energy Resources Technology. Received July 09, 2020;
Accepted manuscript posted September 02, 2020. doi:10.1115/1.4048529
Copyright © 2020 by ASME

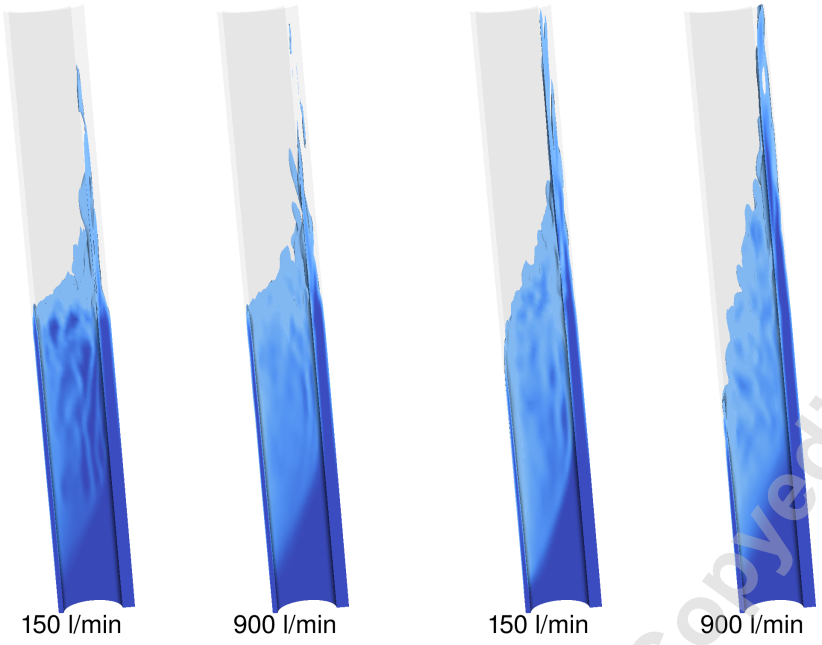

(a) Displaced fluid 1.5 s.g. (b) Displaced fluid 1.8 s.g.

Fig. 11: Snapshots representing the three-dimensional distribution of displacing fluid in a near-vertical regular annulus at $t^* = 0.5$. The shades of blue ranges from volume fraction 10 % as the brightest to 100 % volume fraction of displacing fluid.

In Figs. 13a and 13b we plot the distribution of displacing (blue) fluid at different dimensionless times since start of injection for constant injection rate of 150 l/min. We first note the effect of buoyancy which results in a more horizontal interface between the fluids in Fig. 13a. The fluid interface remains nearly horizontal also above the washout with only a thin finger propagating above the main location of the fluid-fluid interface in Fig. 13a. This is also reflected in the evaluation of non-displaced fluid shown in Fig. 12, where this combination of density differences and flow rate results in the most effective displacement of the four combinations investigated in this paper.

For the simulation summarized in Fig. 13b only one of the ELF design rules was satisfied and we observe a larger axial elongation of the fluid interface now that buoyancy is reduced. Displacing fluid clearly enters the washout through the wide sector of the annulus first. Due to the larger cross-sectional area in the washout, the fluid interface flattens considerably during displacement of the washout. Displacement of the regular section above the washout is similar to that of the regular section below, *i.e.* a fluid interface that elongates axially due to the dominating effect of eccentricity over buoyancy. Both Figs. 12 and 13b suggest poorer displacement of the washout compared to Fig. 13a.

In Figs. 14a and 14b we turn to the higher flow rate of 900 l/min. Starting with Fig. 14a, which is the only combination of density and flow rate that satisfies all four ELF rules in our study, we observe that the fluid distributions are qualitatively similar to that of Fig. 13a, *i.e.* buoyancy is still effective in limiting the axial elongation of the fluid interface. Finally, in Fig. 14b we plot the fluid distributions for the case of high flow rate and small density difference between the two fluids. The trends caused by reduced buoyancy observed in Fig. 13b are now even clearer; displacing fluid enters the washout section

Accepted Manuscript Not Copyedited

Downloaded from http://asmedigitalcollection.asme.org/energyresources/article-pdf/doi/10.1115/1.4048529/6568415/jert-20-1620.pdf by NTNU Universitets Biblioteket user on 25 September 2020

Journal of Energy Resources Technology. Received July 09, 2020;
Accepted manuscript posted September 02, 2020. doi:10.1115/1.4048529
Copyright © 2020 by ASME

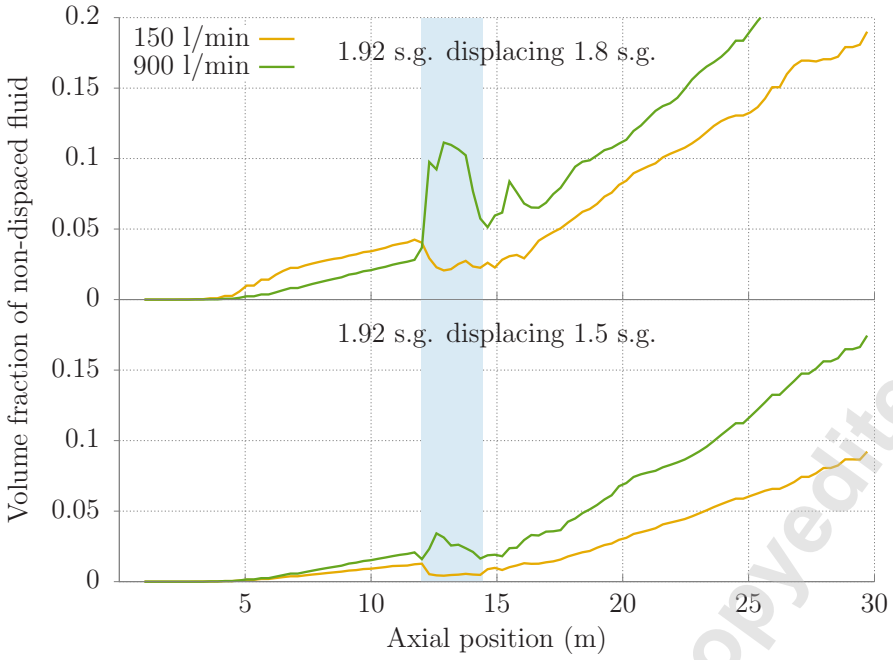

Fig. 12: The cross-sectional average of the non-displaced volume fraction at $t^* = 1$ as a function of the axial position in the model with an irregular section. The density of the displaced fluid is varied between 1.5 s.g. and 1.8 s.g. while the displacing fluid is kept at 1.92 s.g. in all the cases. Two different levels of bulk fluid velocity were simulated as indicated by the curve colors.

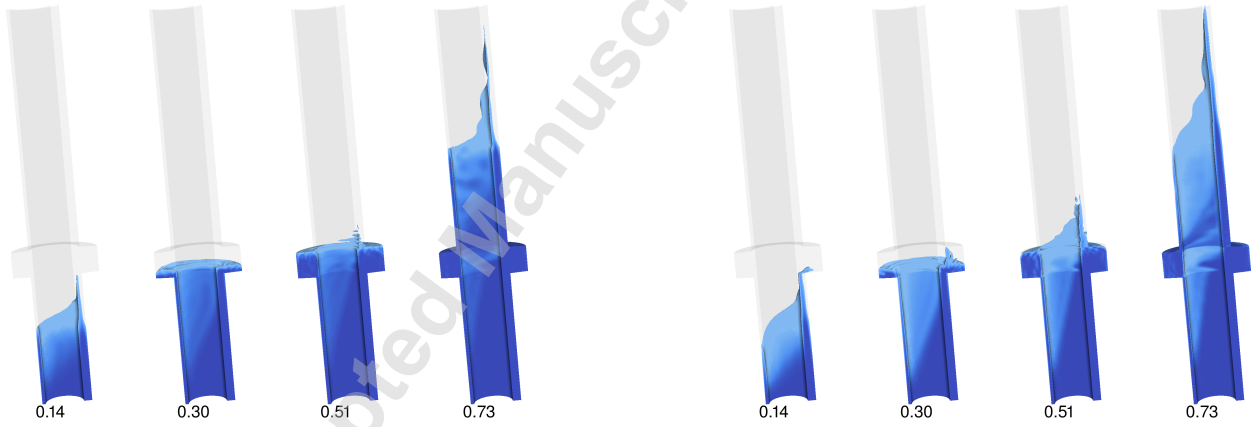

(a) Displaced fluid density 1.5 s.g.

(b) Displaced fluid density 1.8 s.g.

Fig. 13: Snapshots representing the three-dimensional distribution of displacing fluid in a near-vertical annulus at different t^*, as indicated. The shades of blue ranges from volume fraction 10 % as the brightest to 100 % volume fraction of displacing fluid. The injection rate is constant at 150 l/min in both cases.

through the wide sector first and then starts displacing the opposite side of the washout due to density-driven azimuthal flow. Eventually displacing fluid flows into the washout also through the narrow side of the annulus which assists in the overall

Accepted Manuscript Not Copyedited

Downloaded from http://asmedigitalcollection.asme.org/energyresources/article-pdf/doi/10.1115/1.4048529/6568415/jert-20-1620.pdf by NTNU Universitets Biblioteket user on 25 September 2020

Journal of Energy Resources Technology. Received July 09, 2020;
Accepted manuscript posted September 02, 2020. doi:10.1115/1.4048529
Copyright © 2020 by ASME

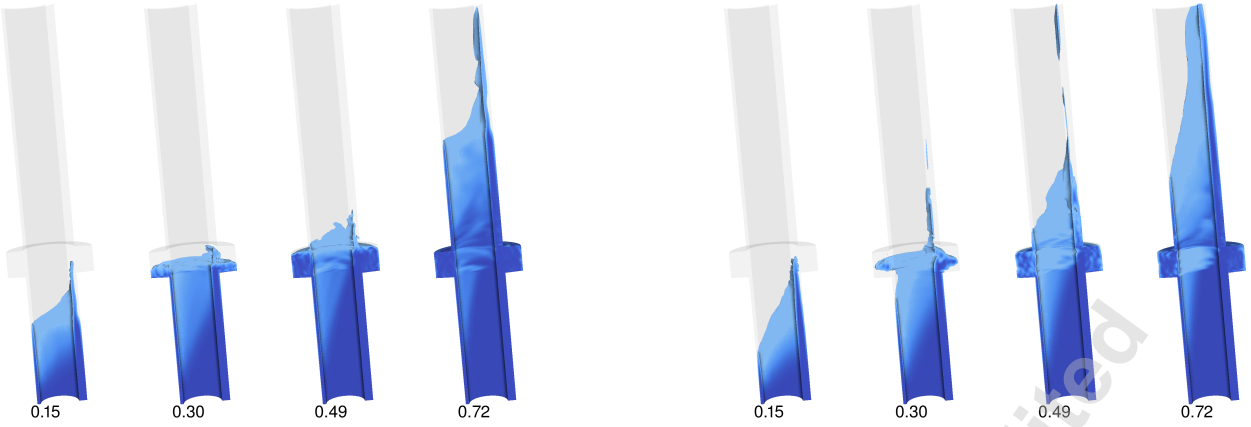

(a) Displaced fluid density 1.5 s.g.

(b) Displaced fluid density 1.8 s.g.

Fig. 14: Snapshots representing the three-dimensional distribution of displacing fluid in a near-vertical annulus at different t^*, as indicated. The shades of blue ranges from volume fraction 10 % as the brightest to 100 % volume fraction of displacing fluid. The injection rate is constant at 900 l/min in both cases.

washout displacement. Displacing fluid enters the regular section above the washout while there are still large pockets of intermixed fluids and residual non-displaced fluid left behind in the washout. Due to the high bulk velocity of the flow and the small mass density difference, the washout is only partly displaced before displacing fluid propagates into the regular section above the washout.

DISCUSSION

The results shown in the previous section suggests that increasing the mass density difference between the displaced and the displacing fluid aids displacement in the near-vertical annulus both in the regular sections below and above the washout and also inside the washout. The results for the regular annulus, presented in Figs. 8, 9 and 10 illustrate the effect of buoyancy on displacement in near-vertical and eccentric annuli; buoyancy promotes a horizontal interface with the denser displacing fluid below the lighter displaced fluid. By reducing the density difference and/or increasing the flow rate, the axial elongation of the interface increases. We also note that the fluid combination that appears to result in the best conditions for displacement in the regular annulus (1.5 s.g. displaced fluid, 150 l/min flow rate) violates the friction pressure hierarchy rule according to the ELF criteria, see Table 4. The large density difference and low flow rate promote piston-like displacements in the eccentric, near-vertical annulus and this most likely outweighs the reversed friction pressure hierarchy between the fluids, resulting in very good overall displacement. Both fluid combinations in the top panel of Fig. 8 violate the differential velocity rule (rule 4 in Table 4); this is manifested in the axial elongation of the fluid interface in these simulations. While the lowest flow rate and the highest density difference results in the best displacement conditions in these purely fluid mechanical simulations, the lower flow rate may not be practical or achievable from an operational perspective. For instance, while injecting dense cement slurry in the casing, undesired free-fall or u-tubing resulting in excessive fluid inter-mixing

Accepted Manuscript Not Copyedited

Downloaded from http://asmedigitalcollection.asme.org/energyresources/article-pdf/doi/10.1115/1.4048529/6568415/jert-20-1620.pdf by NTNU Universitets Biblioteket user on 25 September 2020

Journal of Energy Resources Technology. Received July 09, 2020;
Accepted manuscript posted September 02, 2020. doi:10.1115/1.4048529
Copyright © 2020 by ASME

inside the casing could occur unless a certain minimum injection rate is maintained. Further, a certain minimum wall shear stress may be desired to clean the surfaces of the casing or formation. Similar operational considerations, which are not reflected in the present analysis, may favor overall higher displacement rates.

The examples discussed above show the importance of proper casing centralization on the quality of the displacement, also in the presence of washouts: low density differences and high flow rates can result in unstable displacements and channelling on the wide side of the annulus unless the inner casing is well centralized in the hole. The cases with a heavy displaced fluid (1.8 s.g.) violate at least two of the ELF guidelines for laminar displacement flow, including insufficient density hierarhcy and (related to this) the differential velocity rule. These two cases result in the overall poorest displacements in this study.

Finally, we compare the predicted volume fraction of non-displaced fluid at $t^* = 1$ for the near-vertical annulus in Fig. 12 to the results for the near-horizontal annulus in Ref. [31]. For the regular section below the washout, mass density difference and buoyancy aids displacement in both the near-horizontal and the near-vertical annulus. In the near-horizontal annulus, gravity-assisted slumping of displacing fluid from the upper wide side to the lower narrow side is effective in assisting overall displacement in this regular part of the annulus. Comparing Fig. 12 to Fig. 3 of Ref. [31], we observe very similar volume fractions of residual fluid. The displacement of the washout section is however fairly different for the near-horizontal and the near-vertical annulus. Displacement of the washout is generally better for the near-vertical annulus compared to the near-horizontal annulus since the density difference between the fluids promotes a piston-like displacement of this section with large cross-sectional area. In the near-horizontal annulus, gravity results in slumping of the denser displacing fluid from the upper wide side of the annulus toward the lower side. In the washout in particular, this results in very slow displacement of the lighter from the top part of the washout.

CONCLUSIONS

The effects of flow rate and fluid mass density difference on the displacement quality in a regular and an irregular near-vertical annulus has been the focus of this paper. Primary cementing of liners and casing strings is the industrial operation that motivates our study. As such, we have analyzed four combinations of fluid mass densities and flow rates and compared these combinations to industry guidelines for effective laminar flow. These guidelines were developed and designed to promote stable laminar displacements in generally eccentric annuli, and we find that only one out of the four combinations of densities and flow rates satisfies all four guidelines simultaneously. The overall best displacement quality of both the regular and the irregular annulus is achieved with the largest mass density contrast and the lowest flow rate. This combination (which in fact violates the friction pressure hierarchy guideline) results in piston-like displacement where the large buoyancy force is effective in producing a nearly horizontal interface between the fluids in the regular and in the irregular sections. While the lowest flow rate and the highest density difference results in apparently better displacement conditions in these simulations, we point out that the lower flow rate may not be practical or achievable from an operational perspective. We observe stable displacement of the washout with minimal intermixing between fluids for this specific case, which also benefits the displacement quality of the regular section above the washout. When the displaced fluid is just

Accepted Manuscript Not Copyedited

Downloaded from http://asmedigitalcollection.asme.org/energyresources/article-pdf/doi/10.1115/1.4048529/6568415/jert-20-1620.pdf by NTNU Universitets Biblioteket user on 25 September 2020

Journal of Energy Resources Technology. Received July 09, 2020;
Accepted manuscript posted September 02, 2020. doi:10.1115/1.4048529
Copyright © 2020 by ASME

slightly less dense than the displacing fluid, the stabilizing effect of buoyancy is reduced and eccentricity of the inner string leads to an axially elongated interface between the fluids even at low flow rates. The combination of low density difference and high flow rate leads to unstable displacements - the presence of washouts can in such cases exacerbate the situation further by increasing intermixing of fluids. Our main observations are qualitatively consistent with recent simulations of annular displacement outside vertical surface casings [32]. When comparing with previous results for a near-horizontal irregular annulus [31], we observe that the inclination is important for the displacement efficiency and location of residual fluids inside the washout. The effects of fluid intermixing inside the washout and possible implications for the cement quality above the washout remain uncertain however, and is considered as a possible topic for future research.

Acknowledgements

The Research Council of Norway, ConocoPhillips, AkerBP, Equinor and Wintershall are acknowledged for financing the work through PETROMAKS2 project number 244577 and the research centre DrillWell - Drilling and Well Centre for Improved Recovery, a research cooperation between NORCE, NTNU, SINTEF and UiS. The numerical simulations were completed with funding from the Research Council of Norway through PETROMAKS2 project number 294815 and performed on resources provided by UNINETT Sigma2 - the National Infrastructure for High Performance Computing and Data Storage in Norway.

Nomenclature

g Gravitational acceleration [m/s^2]

h Radial gap width [m]

K Consistency index [Pa·s^n]

n Shear thinning index

p Pressure [Pa]

Q Volumetric flow rate [m^3/s]

t Time [s]

t^* Dimensionless time $(= Qt/V)$

u Velocity vector [m/s]

V Annulus volume [m^3]

β Inclination from vertical [radians]

$\dot{\boldsymbol{\gamma}}$ Rate of strain tensor [s^{-1}]

$\dot{\gamma}$ Shear rate [s^{-1}]

ρ Mass density [kg/m^3]

$\boldsymbol{\tau}$ Deviatoric stress tensor [Pa]

τ Shear stress [Pa]

Accepted Manuscript Not Copyedited

Downloaded from http://asmedigitalcollection.asme.org/energyresources/article-pdf/doi/10.1115/1.4048529/6568415/jert-20-1620.pdf by NTNU Universitets Biblioteket user on 25 September 2020

Journal of Energy Resources Technology. Received July 09, 2020;
Accepted manuscript posted September 02, 2020. doi:10.1115/1.4048529
Copyright © 2020 by ASME

τ_y Yield stress [Pa]

μ Viscosity [Pa·s]

References

[1] Nelson, E. B., and Guillot, D., eds., 2006. Well Cementing, 2 ed. Schlumberger, Sugar Land, Texas, US.

[2] Walton, I. C., and Bittleston, S. H., 1991. "The axial flow of a Bingham plastic in a narrow eccentric annulus". J. Fluid Mech., **222**, January, pp. 39 – 60.

[3] Szabo, P., and Hassager, O., 1992. "Flow of viscoplastic fluids in eccentric annular geometries". J. Non-Newtonian Fluid Mech., **45**(2), November, pp. 149 – 169.

[4] Agbasimalo, N., and Radonjic, M., 2014. "Experimental Study of the Impact of Drilling Fluid Contamination on the Integrity of Cement-Formation Interface". ASME J. Energy Resour. Technol, **136**, p. 042908.

[5] Haciislamoglu, M., and Langlinais, J., 1990. "Non-Newtonian Flow in Eccentric Annuli". ASME J. Energy Resour. Technol, **112**, pp. 163 – 169.

[6] Hussain, Q. E., and Sharif, M. A. R., 1998. "Analysis of Yield-Power-Law Fluid Flow in Irregular Eccentric Annuli". ASME J. Energy Resour. Technol, **120**, pp. 201–207.

[7] McLean, R. H., Manry, C. W., and Whitaker, W. W., 1967. "Displacement Mechanics in Primary Cementing". Journal of Petroleum Technology, **19**(02), pp. 251–260. SPE 1488.

[8] Clark, C. R., and Carter, G. L., 1973. "Mud Displacement with Cement Slurries". Journal of Petroleum Technology, **25**(7), July, pp. 775 – 783. SPE 4090.

[9] Lockyear, C. F., and Hibbert, A. P., 1989. "Integrated Primary Cementing Study Defines Key Factors for Field Success". Journal of Petroleum Technology, **41**(12), December, pp. 1320 – 1325. SPE 18376.

[10] Guillot, D. J., Froelich, B., Caceres, E., and Verbakel, R., 2008. "Are Casing Centralization Calculations Really Conservative?". In IADC/SPE Drilling Conference, Orlando, Florida, USA, 4-6 March, pp. 1–11. IADC/SPE 112725.

[11] Jakobsen, J., Sterri, N., Saasen, A., Aas, B., Kjosnes, I., and Vigen, A., 1991. "Displacements in Eccentric Annuli During Primary Cementing in Deviated Wells". In SPE Production Operations Symposium, 7-9 April, Society of Petroleum Engineers. SPE 21686.

[12] Tehrani, M. A., Bittleston, S. H., and Long, P. J. G., 1993. "Flow instabilities during annular displacement of one non-Newtonian fluid by another". Experiments in Fluids, **14**(4), February, pp. 246 – 256.

[13] Malekmohammadi, S., Carrasco-Teja, M., Storey, S., Frigaard, I. A., and Martinez, D. M., 2010. "An experimental study of laminar displacement flows in narrow vertical eccentric annuli". Journal of Fluid Mechanics, **649**, 4, pp. 371–398.

[14] Couturier, M., Guillot, D., Hendriks, H., and Callet, F., 1990. "Design Rules And Associated Spacer Properties For Optimal Mud Removal In Eccentric Annuli". In CIM/SPE International Technical Meeting, pp. 1–8. SPE 21594.

[15] Théron, B. E., Bodin, D., and Fleming, J., 2002. "Optimization of Spacer Rheology Using Neural Network Technology". In IADC/SPE Drilling Conference, pp. 1–8. IADC/SPE 74498.

Accepted Manuscript Not Copyedited

Downloaded from http://asmedigitalcollection.asme.org/energyresources/article-pdf/doi/10.1115/1.4048529/6568415/jert-20-1620.pdf by NTNU Universitets Biblioteket user on 25 September 2020

Journal of Energy Resources Technology. Received July 09, 2020;
Accepted manuscript posted September 02, 2020. doi:10.1115/1.4048529
Copyright © 2020 by ASME

[16] Pelipenko, S., and Frigaard, I. A., 2004. "Visco-plastic fluid displacements in near-vertical narrow eccentric annuli: prediction of travelling-wave solutions and interfacial instability". J. Fluid Mech., **520**, pp. 343–377.

[17] Bittleston, S. H., Ferguson, J., and Frigaard, I. A., 2002. "Mud removal and cement placement during primary cementing of an oil well – Laminar non-Newtonian displacements in an eccentric annular Hele-Shaw cell". Journal of Engineering Mathematics, **43**(2), pp. 229–253.

[18] Plácido, J. C. R., Santos, H. M. R., and Galeano, Y. D., 2002. "Drillstring vibration and wellbore instability". J. Energy Resour. Technol., **124**(4), pp. 217–222.

[19] Skadsem, H. J., Saasen, A., and Håvardstein, S., 2017. "Casing centralization in irregular wellbores". In Proceedings of the ASME 2018 36th International Conference on Ocean, Offshore and Arctic Engineering, Trondheim, Norway, pp. 1–10. OMAE2017-61106.

[20] Fjær, E., Holt, R. M., Nes, O.-M., and Sønstebø, E. F., 2002. "Mud Chemistry Effects on Time-Delayed Borehole Stability Problems in Shales". SPE/ISRM Rock Mechanics Conference, 20-23 October, Irving, Texas(SPE 78163), October.

[21] Nes, O. M., Fjær, E., Tronvoll, J., Kristiansen, T. G., and Horsrud, P., 2012. "Drilling Time Reduction Through an Integrated Rock Mechanics Analysis". ASME J. Energy Resour. Technol, **134**, p. 032802.

[22] Roustaei, A., and Frigaard, I. A., 2013. "The occurrence of fouling layers in the flow of a yield stress fluid along a wavy-walled channel". J. Non-Newt. Fluid Mech., **198**, pp. 109 – 124.

[23] Roustaei, A., Gosselin, A., and Frigaard, I. A., 2015. "Residual drilling mud during conditioning of uneven boreholes in primary cementing. Part 1: Rheology and geometry effects in non-inertial flows". J. Non-Newt. Fluid Mech., **220**(87 - 98).

[24] Roustaei, A., and Frigaard, I. A., 2015. "Residual drilling mud during conditioning of uneven boreholes in primary cementing. Part 2: Steady laminar inertial flows". J. Non-Newt. Fluid Mech., **226**(1 - 15).

[25] Zuiderwijk, J. J. M., 1974. "Mud Displacement In Primary Cementation". In SPE European Spring Meeting, 29-30 May, Society of Petroleum Engineers. SPE 4830.

[26] Kimura, K., Takase, K., Griffith, J. E., Gibson, R. A., Porter, D. S., and Becker, T. E., 1999. "Custom-Blending Foamed Cement for Multiple Challenges". In SPE/IADC Middle East Drilling Technology Conference, 8-10 November, Society of Petroleum Engineers. SPE 57585.

[27] Skadsem, H. J., Kragset, S., and Sørbø, J., 2019. "Cementing an Irregular Annulus Geometry: Full-Scale Experiments and 3D Simulations". In SPE/IADC Drilling Conference and Exhibition, 5-7 March 2019, The Hague, The Netherlands, pp. 1–15. SPE/IADC 194091.

[28] Lund, B., Ytrehus, J. D., Taghipour, A., Divyankar, S., and Saasen, A., 2018. "Fluid-fluid displacement for primary cementing in deviated washout sections". In Proceedings of the ASME 2018 37th International Conference on Ocean, Offshore and Arctic Engineering, Madrid, Spain, pp. 1–9. OMAE2018-78707.

[29] Renteria, A., Maleki, A., Frigaard, I. A., Lund, B., Taghipour, A., and Ytrehus, J. D., 2019. "Effects of irregularity on displacement flows in primary cementing of highly deviated wells". J. Petrol. Sci. Eng., **172**, pp. 662–680.

Accepted Manuscript Not Copyedited

Downloaded from http://asmedigitalcollection.asme.org/energyresources/article-pdf/doi/10.1115/1.4048529/6568415/jert-20-1620.pdf by NTNU Universitets Biblioteket user on 25 September 2020

Journal of Energy Resources Technology. Received July 09, 2020;
Accepted manuscript posted September 02, 2020. doi:10.1115/1.4048529
Copyright © 2020 by ASME

[30] Skadsem, H. J., Kragset, S., Lund, B., Ytrehus, J. D., and Taghipour, A., 2019. "Annular displacement in a highly inclined irregular wellbore: Experimental and three-dimensional numerical simulations". J. Petrol. Sci. Eng., **172**, pp. 998–1013.

[31] Kragset, S., and Skadsem, H. J., 2018. "Effect of Buoyancy and Inertia on Viscoplastic Fluid: Fluid Displacement in an Inclined Eccentric Annulus With an Irregular Section". In ASME 2018 37th International Conference on Ocean, Offshore and Arctic Engineering, Vol. 8: Polar and Arctic Sciences and Technology: Petroleum Technology, pp. 1–10. OMAE2018-77519.

[32] Etrati, A., Roustaei, A., and Frigaard, I. A., 2020. "Strategies for mud-removal from washouts during cementing of vertical surface casing". Journal of Petroleum Science and Engineering, July, p. 107454. In press.

[33] Aas, B., Sørbø, J., Stokka, S., Saasen, A., Godøy, R., Lunde, Ø., and Vrålstad, T., 2016. "Cement Placement with Tubing Left in Hole during Plug and Abandonment Operations". In IADC/SPE Drilling Conference and Exhibition, 1-3 March, Fort Worth, Texas, USA, pp. 1–13. IADC/SPE 178840.

[34] OpenFOAM. http://www.openfoam.org.

[35] Papanastasiou, T. C., 1987. "Flows of Materials with Yield". Journal of Rheology, **31**(5), pp. 385–404.

[36] Hanks, R. W., 1979. "The Axial Laminar Flow of Yield-Pseudoplastic Fluids in a Concentric Annulus". Ind. Eng. Chem. Process Des. Dev., **18**(3), pp. 488 – 493.

[37] Tehrani, A., Ferguson, J., and Bittleston, S. H., 1992. "Laminar Displacement in Annuli: A Combined Experimental and Theoretical Study". In SPE Annual Technical Conference and Exhibition, 4-7 October, Society of Petroleum Engineers. SPE 24569.

[38] Tardy, P. M. J., and Bittleston, S. H., 2015. "A model for annular displacements of wellbore completion fluids involving casing movement". Journal of Petroleum Science and Engineering, **126**, pp. 105–123.

List of Tables

List of Figures

Accepted Manuscript Not Copyedited

Downloaded from http://asmedigitalcollection.asme.org/energyresources/article-pdf/doi/10.1115/1.4048529/6568415/jert-20-1620.pdf by NTNU Universitets Biblioteket user on 25 September 2020

Journal of Energy Resources Technology. Received July 09, 2020;
Accepted manuscript posted September 02, 2020. doi:10.1115/1.4048529
Copyright © 2020 by ASME

Accepted Manuscript Not Copyedited

Downloaded from http://asmedigitalcollection.asme.org/energyresources/article-pdf/doi/10.1115/1.4048529/6568415/jert-20-1620.pdf by NTNU Universitets Biblioteket user on 25 September 2020

Journal of Energy Resources Technology. Received July 09, 2020;
Accepted manuscript posted September 02, 2020. doi:10.1115/1.4048529
Copyright © 2020 by ASME

Downloaded from http://asmedigitalcollection.asme.org/energyresources/article-pdf/doi/10.1115/1.4048529/6568415/jert-20-1620.pdf by NTNU Universitets Biblioteket user on 25 September 2020

Accepted Manuscript Not Copyedited